Cylindrically shaped zinc-blende semiconductor quantum dots do not have cylindrical symmetry: Atomistic symmetry, atomic relaxation, and piezoelectric effects

Gabriel Bester and Alex Zunger
National Renewable Energy Laboratory, Golden, Colorado 80401, USA
(Received 1 April 2004; published 14 January 2005)

Self-assembled quantum dots are often modeled by continuum models (effective mass or $\mathbf{k}\cdot\mathbf{p}$) that assume the symmetry of the dot to be that of its overall geometric shape. Lens-shaped or conical dots are thus assumed to have continuous cylindrical symmetry $C_{\infty v}$, whereas pyramidal dots are assumed to have C_{4v} symmetry. However, considering that the III–V dots are made of atoms arranged on the (relaxed) positions of a zinc-blende lattice, one would expect the highest possible symmetry in these structures to be C_{2v}. In this symmetry group all states are singly degenerate and there are no *a priori* reason to expect, e.g., the electron *P* states (usually the second and third electron levels of dominant orbital *P* character) to be degenerate. Continuum models, however, predict these states to be energetically degenerate unless an irregular shape is postulated. We show that, in fact, the true (atomistic) symmetry of the dots is revealed when the effects of (i) interfacial symmetry, (ii) atomistic strain, and (iii) piezoelectricity are taken into account. We quantify the contributions of each of these effects separately by calculating the splitting of electron *P* levels for different dot shapes at different levels of theory. We find that for an ideal square-based pyramidal InAs/GaAs dot the interfacial symmetry of the unrelaxed dot splits the *P* level by 3.9 meV, atomistic relaxation adds a splitting of 18.3 meV (zero if continuum elasticity is used to calculate strain) and piezoelectricity reduces the splitting by -8.4 meV, for a total splitting of 13.8 meV. We further show that the atomistic effects (i) and (ii) favor an orientation of the electron wave functions along the $[1\bar{1}0]$ direction while effect (iii) favors the $[110]$ direction. Whereas effects (i) + (ii) prevail for a pyramidal dot, for a lens shaped dot, effect (iii) is dominant. We show that the 8–band $\mathbf{k}\cdot\mathbf{p}$ method, applied to pyramidal InAs/GaAs dots describes incorrectly the splitting and order of *P* levels (–9 meV instead of 14 meV splitting) and yields the orientation $[110]$ instead of $[1\bar{1}0]$.

DOI: 10.1103/PhysRevB.71.045318 PACS number(s): 73.21.La, 71.15.−m, 73.22.Dj

I. INTRODUCTION: WHY DO DOTS HAVE LOWER

such symmetry lowering exists already for ideally shaped dots, e.g., perfect square-based pyramid with zincblende structure. The classic effective-mass and $\mathbf{k}\cdot\mathbf{p}$ treatment of nanostructures[9,11] neglects all three effects giving rise to unsplit P and D states and unpolarized inter- and intraband transitions. A possible cure to the lack of polarization anisotropies and simplified photoluminescence spectra of the continuum methods was given in the works of Stier, Grundmann, and Bimberg,[22–24] Pryor,[25] and Hackenbuchner *et al.*[26]

$$\rho_{\text{piezo}}(\mathbf{r}) = -\nabla \cdot \mathbf{P} = -\nabla \cdot \begin{Bmatrix} e_{14}(\mathbf{r})\{\epsilon_{yz}(\mathbf{r}) + \epsilon_{zy}(\mathbf{r})\} \\ e_{14}(\mathbf{r})\{\epsilon_{zx}(\mathbf{r}) + \epsilon_{xz}(\mathbf{r})\} \\ e_{14}(\mathbf{r})\{\epsilon_{xy}(\mathbf{r}) + \epsilon_{yx}(\mathbf{r})\} \end{Bmatrix}. \tag{5}$$

The divergence is calculated using a piecewise polynomial function to represent the polarization data points.[44]

In the last step the piezoelectric potential V_{piezo} is obtained from the Poisson equation

$$\rho_{\text{piezo}}(\mathbf{r}) = \epsilon_0 \nabla \cdot \{\epsilon_s(\mathbf{r}) \nabla V_{\text{piezo}}(\mathbf{r})\}. \tag{6}$$

The piezoelectric density ρ_{piezo} is thereby expanded in multipoles up to a certain angular momentum to obtain the accurate boundary conditions for the long-ranged potential. The Poisson equation is then solved using a conjugate gradient algorithm finding the piezopotential $V_{\text{piezo}}(\mathbf{r})$. Particular care has been taken for the numerical differentiation where basic finite difference methods have been tested against polynomial interpolations. While the results of both approaches are in excellent agreement, the convergence of the conjugate gradient algorithm is most stable with polynomials of third order.[44] For grid sizes of $80\times80\times80$ the result is usually obtained in a dozen iterations within a few minutes of computational time on a standard personal computer.

Once the total potential $\Sigma_{n\alpha}[v_\alpha(\mathbf{r}-\mathbf{R}_n)+\hat{v}_\alpha^{SO}]+V_{\text{piezo}}(\mathbf{r})$ is defined, the basis set has to be chosen. The single-particle dot wave functions are expanded in terms of strain-dependent Bloch functions $\psi_i=\Sigma A_{n,\mathbf{k}}\varphi_{n,\mathbf{k}}(r)$ of band index n and wave vector $\mathbf{k}$ of the underlying bulk solids. In this "linear combination of bulk bands" approach,[45] basis functions are obtained throughout the Brillouin zone and differ in this respect from the $\mathbf{k}\cdot\mathbf{p}$ method. This results in a far greater[46] variational accuracy, and incorporates naturally both intervalley (e.g., $\Gamma-X-L$) and multiband (various n's) couplings. The ladder of electron (hole) single-particle states will be denoted as $e_0,e_1,e_2,\ldots$ $(h_0,h_1,h_2,\ldots)$ for ground state, first excited state, etc.

III. EFFECTS REVEALING THE ATOMISTIC SYMMETRY OF THE NANOSTRUCTURE

In this section we will discuss the three distinct physical effects responsible for the lowering of the symmetry, starting from the continuum-like symmetry and progressing to the true atomistic symmetry. In order to quantify the importance of these effects, we will present specific results on the splitting of the single-particle electron P states. In a continuum-like description these states are exactly degenerate and their wave functions are isotropic in the (001) plane. On the other hand, the fully atomistic description of a cylindrical, lens shaped or pyramidal dot yields split P states with well defined wave function orientation, either along the [110] or the $[1\bar{1}0]$ directions. We will report on the energetic splitting $\Delta E=\varepsilon_{[110]}-\varepsilon_{[1\bar{1}0]}$ where $\varepsilon_{[110]}$ $(\varepsilon_{[1\bar{1}0]})$ is the single particle energy of the electron state oriented along the [110] $([1\bar{1}0])$ direction for different dot shapes and sizes, given in Fig. 1. We consider a set of dots with a common base dimension of 11.3 nm and different shapes and sizes: a disk with 4.6 nm height, a truncated cone with a top base of 2.3 nm, and a height of 4.6 nm, a pyramid with a height of 5.6 nm ({101} side facets), a lens with 4.6 nm height. In addition we calculated sizes that are more realistic,[3,4] namely a set of lenses with 25.2 nm base and four different heights (3.5, 5.0, 5.5, 6.5 nm). To isolate the physical factors responsible for level splitting and wave function anisotropy of dots with ideal shape symmetry we distinguish four levels of theory, starting from the simplest. While there are other ways of separating the various effects, the partitioning below is a convenient way to isolate the main physical effects of chemical symmetry, short-ranged relaxation and long-ranged strain fields.

Level 1: The symmetry of the nanostructure is taken as the shape symmetry; so a pyramid is assumed to have C_{4v} symmetry, a lens, disk, or truncated cone has $C_{\infty v}$ symmetry. Strain is taken into account by continuum elasticity, or neglected. Piezoelectricity is neglected. This is the approach taken by classical effective mass[13] or $\mathbf{k}\cdot\mathbf{p}$[9–11] approaches.

Level 2: The nanostructure is constructed from atoms and has therefore C_{2v} symmetry. In this level, however, InAs dot and the GaAs matrix both have the lattice positions of per-

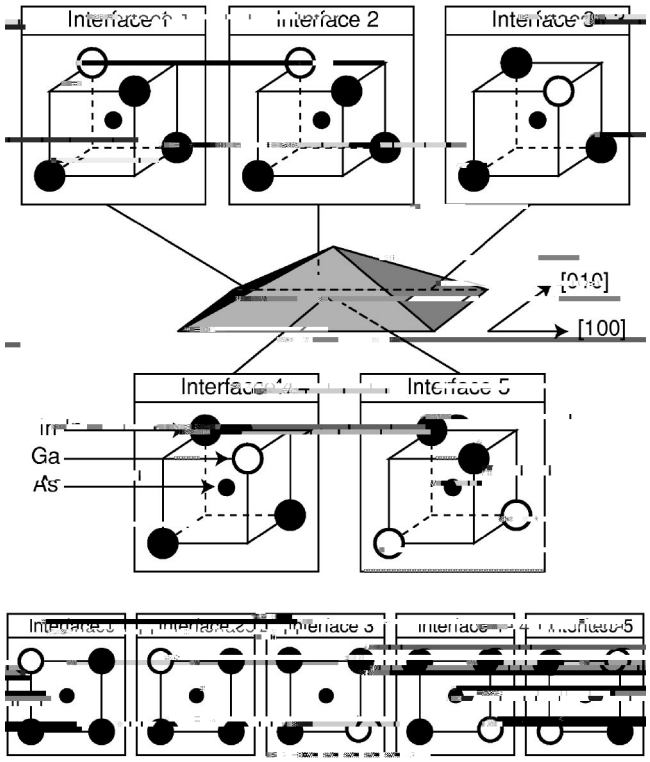

FIG. 2. Atomistic detail of the interfaces of a square-based InAs pyramid with base b and height $b/2$, embedded in GaAs. The zinc-blende unit cells give the atomic arrangement in the direct vicinity of the interface. At the bottom of the figure a top view of the interfaces is given.

tively) of a square-based pyramid are analyzed. For the (001) interface at the base of the pyramid (Fig. 2 interface 5) the [110] and $[1\bar{1}0]$ directions are inequivalent. Even for a common anion quantum dot/barrier nanostructure (e.g., InAs/GaAs) the anion plane at interface 5 is anisotropic. The direct neighbors *above* the anion plane (In atoms) that align in the $[\bar{1}10]$ direction are chemically different from the neighbors *under* the anion plane (Ga atoms) that align in the [110] direction. Similar observations can be made for all facets of the pyramid and most relevant is the fact that these effects do not compensate each other. At the bottom of Fig. 2 a top view of the zinc-blende unit cells shows that even after the summation of the 1–4 interfaces a net anisotropy remains at the As site.

The effect of the atomistic interface symmetry on the potential of Eq. (1) can be seen in Fig. 3(a) which shows the difference between the pseudopotential $\Sigma_\alpha v_\alpha(\mathbf{r}-\mathbf{R}_\alpha)$ along the [110] and $[1\bar{1}0]$ directions for an *unrelaxed* square-based pyramid without piezoeffect. The potential has been averaged in [001] direction over two unit cells centered 1 nm above the base of the pyramid.[64] Figure 3(a) shows that the differences between the atomic pseudopotentials in [110] and $[1\bar{1}0]$ directions are well localized at the interfaces (shown as shaded areas marked InGaAs) and vanishes inside the nanostructure.

The first line in Table I shows the magnitude of the atomistic interface effect on the P-level splitting for different shapes and sizes (see Fig. 1 to visualize the geometries). We

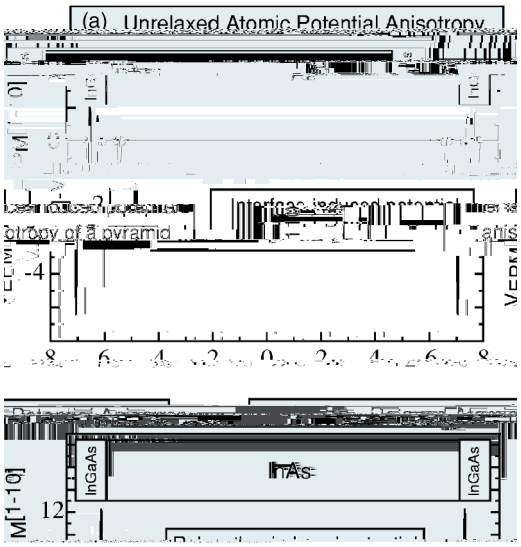

FIG. 3. (a) Difference between the atomistic pseudopotential in [110] and $[1\bar{1}0]$ directions for an *unrelaxed* square-based pyramid with 11.3 nm base and 5.6 nm height. The potential has been averaged in [001] direction over two unit cells centered 1 nm above the base of the pyramid. The position of the interfaces are shown as shaded areas labeled InGaAs. (b) Same as (a) for the *relaxed* square-based pyramid. (c) Difference between the piezoelectric potential [using the bulk values of $e_{14}(\mathrm{InAs})=-0.045\ \mathrm{C/m^2}$ and $e_{14}(\mathrm{GaAs})=-0.16\ \mathrm{C/m^2}$] in [110] and $[1\bar{1}0]$ directions for the relaxed square-based pyramid.

see in Table I that the interface effect is strongest for the pyramid, having sharply defined facets; this effect splits the electron P states by 3.9 meV. For a truncated cone where the only sharp interfaces are the base and the top, the splitting is smaller, but still 2.3 meV. The two large lenses have a small splitting of 0.5 and 0.4 meV which could be attributed to the fact that the confined states make less "contact" with the interface in a larger structure. The disk has small splitting of 0.1 meV for symmetry reasons: with no vertical facets but

with two (001) interfaces the effects from both interfaces compensate each other and yield wave functions (not shown) isotropic in the (001) plane with D_{2d} symmetry and no splitting of the electron P states. This effect is similar to the one well known for symmetric quantum wells.[47]

The interfacial symmetry affects the wave functions. The envelope functions for the first electron P state of the pyramid, the truncated cone and the lens are oriented along the $[1\bar{1}0]$ direction, whereas the *second* state is oriented along the $[110]$ direction. The wave function orientation is given by the sign of ΔE and explicitely denoted in Table I as $[110]$ or $[1\bar{1}0]$ or [iso] (isotropic). The interface effect discussed here is not accounted for by *Level 1* theories based on continuum elasticity (e.g., effective mass models)[13] since the symmetry of the continuum mechanical strain tensor in the (001) plane is C_{4v} so the strain components are equal along the $[110]$ and $[\bar{1}10]$ directions. Such theories produce a vanishing splitting of the electron P states.

B. Atomic relaxation effects: Level 3 versus Level 2

When the atoms are allowed to react to the stress present in all lattice-mismatched self-assembled quantum dots, the interface anisotropy propagates into the interior of the nanostructure. This can be seen in Fig. 3(b) where the difference between the relaxed atomistic potential $\Sigma_\alpha v_\alpha(\mathbf{r}-\mathbf{R}_n)$ along $[110]$ and $[1\bar{1}0]$ directions is plotted (without piezoelectric effect). The effect of the interface now penetrates the nanostructure and has a net effect inside the pyramid, directly affecting the main confinement volume.

A further effect contributes to the anisotropy: In a dot of typical shape, where the base is larger than the top, there is a gradient in the magnitude of the strain tensor between top and bottom. Figure 4 shows this gradient for the hydrostatic strain (the trace of the strain tensor) of a pyramidal quantum dot. Each anion in the dot has two cation neighbors above, oriented along the $[110]$ direction, and two cation neighbors below, oriented along the $[1\bar{1}0]$ direction. The cations above (along $[110]$) experience therefore systematically more stress than the cations below (along $[1\bar{1}0]$) making these directions inequivalent.

The magnitude of the stress relaxation effects on the P-level splitting can be seen in the second line of Table I for different dot shapes. For the pyramid, with strong interface anisotropy and the largest height, the atomic relaxation effect is the strongest being 18.3 meV. For the disk, where strain gradient an interface anisotropy are absent, this effect is zero. The truncated cone exhibits also a noticeable splitting of

the piezoelectric effect in dots.[22,24,25,57] Thus, in what follows we will first assume the piezoelectric constant of InAs to be the one of the bulk and then, examine the piezoelectric effect using a *range* of InAs e_{14} values.

Figure 3(c) shows the difference between the piezoelectric potential $V_{\text{piezo}}(\mathbf{r})$ along the $[110]$ and $[1\bar{1}0]$ directions of the square-based pyramid using the bulk values e_{14}(InAs) and e_{14}(GaAs). A three dimensional plot for the piezoelectric potential with isosurfaces for potential values of $+30$ and -30 mV is given in Fig. 9(a) for a lens shaped quantum dot. The strongest piezoelectric potential is located outside the nanostructure where the piezoelectric constant is largest and near the interface in regions of highest strain. The piezoelectric field in the region where the states are confined, inside the

mid and the truncated cone, piezoelectricity reduces the splitting without changing its sign. For the 5.5 and 3.5 nm tall lenses, however, the piezoelectric effect has larger magnitude than the sum of interface and stress relaxation, and it determines the final orientation of the electron P states. For the most realistic flatter lens of 3.5 nm, the total P-level splitting is -0.5 meV, and the portion due to piezoelectricity is comparable to the one due to interface and stress relaxation.

The effect of piezoelectricity on the wave functions of the flat lens (lens 3) can be seen in the lower half of Fig. 5. In level 4 (with piezoelectricity) the first electron P state e_1 is now oriented along the $[110]$ direction whereas in *Level 3* (without piezoelectricity) it was oriented along the $[1\bar{1}0]$ direction. For the lens shaped dot, the second P-level (e_2) was oriented along the $[1\bar{1}0]$ direction without piezoelectricity but it rotates to the $[110]$ direction when piezoelectricity is considered. In contrast, for the pyramid and the truncated cone the first electron P-state e_1 remain oriented along the $[1\bar{1}0]$ direction in *Level 4* after taking piezoelectricity into account. This can be seen for the pyramid in Fig. 6 that shows the first three electron and hole wave functions squared with and without piezoelectricity. The electron states do not change orientation since the atomistic strain effect of level-2 (that favors $[1\bar{1}0]$ orientation for electrons) is stronger than the piezoelectric effect (that favors $[110]$ orientation). The piezoelectric field makes the orientation of the holes along the $[110]$ direction less favorable. The third hole state h_2

As noted earlier, the quantum dot is under significant compressive strain (Fig. 8) and the value of the piezoelectric constant e_{14}(InAs) is likely to differ (Fig. 7) from the unstrained bulk value assumed so far. To estimate the effect of the choice of e_{14}(InAs) we performed pseudopotential calculations of the electron states for the following values of e_{14}(InAs) inspired from Fig. 7: {)

for h_0 and h_1 and mainly at the tip and along the [110] direction for the state h_2. For the lens shape, we agree with previous EPM results[38,63] to within 0.6 meV. Atomistic interface and strain effects favors the $[1\bar{1}0]$ direction for both the electrons and the holes.

(ii) *With piezoelectricity*: Our results for the pyramid disagree with $\mathbf{k}\cdot\mathbf{p}$ in wave function orientation (see Fig. 6) and in *P*-level splitting (13.8 vs -9 meV). Also, in the $\mathbf{k}\cdot\mathbf{p}$ approximation the effect of piezoelectricity is to rotate the e_1 and e_2 wave functions by 90 deg where no such rotation exists in the atomistic approach which gives the correct orientation both, with and without piezoelectric effect. The reason for the disagreement is the missing atomistic splitting of 22 meV in $\mathbf{k}\cdot\mathbf{p}$. Piezoelectricity favors the [110] direction for electrons and the $[1\bar{1}0]$ direction for holes while atomistic features (levels 2 and 3) favor the $[1\bar{1}0]$ direction for both electrons and holes. For the pyramid the atomistic effects of *levels 2* and *3* prevail and the first electron *P* state is oriented along the $[1\bar{1}0]$. The hole wave function orientation as given by the atomistic and by the $\mathbf{k}\cdot\mathbf{p}$ method agrees for states *h*

[1] N. Liu, J. Tersoff, O. Baklenov, A. L. Holmes, and C. K. Shih, Phys. Rev. Lett. **84**, 334 (2000).
[2] P. Crozier, M. Catalano, R. Cingolani, and A. Passaseo, Appl. Phys. Lett. **79**, 3170 (2001).
[3] T. Walther, A. G. Cullis, D. J. Norris, and M. Hopkinson, Phys. Rev. Lett. **86**, 2381 (2001).
[4] R. Kegel, T. H. Metzger, A. Lorke, J. Peisl, J. Stangl, G. Bauer, K. Nordlund, W. V. Schoenfeld, and P. M. Petroff, Phys. Rev. B **63**, 035318 (2001).
[5] K. Yamaguchi, Y. Saito, and R. Ohtsubo, Appl. Surf. Sci. **190**, 212 (2002).
[6] D. Bruls, J. Vugs, P. Koenraad, H. Salemink, J. Wolter, M. Hopkinson, M. Skolnick, F. Long, and S. Gill, Appl. Phys. Lett. **81**, 1708 (2002).
[7] U. Woggon, *Optical Properties of Semiconductor Quantum Dots* (Springer-Verlag, Berlin, 1997).
[8] D. Bimberg, M. Grundmann, and N. N. Ledentsov, *Quantum Dots Heterostructures* (Wiley, New York, 1999).
[9] E. O. Kane, *Handbook on Semiconductors* (North Holland, Amsterdam, 1982), Vol. 1.
[10] M. Altarelli, *Band Structure, Impurities and Excitons in Superlattices, Heterojunctions and Semiconductor Superlattices* (Springer, Berlin, 1986).
[11] G. Bastard, *Wave Mechanics Applied to Semiconductor Heterostructures* (Halstead, New York, 1988).
[12] J. Marzin and G. Bastard, Solid State Commun. **92**, 437 (1994).
[13] L. Jacak, P. Harylak, and A. Wójs, *Quantum Dots* (Springer-Verlag, Berlin, 1998).
[14] M. Koskinen, S. M. Reimann, and M. Manninen, Phys. Rev. Lett. **90**, 066802 (2003).
[15] D. Ceperley, Rev. Mod. Phys. **67**, 279 (1995).
[16] M. Sugisaki, H.-W. Ren, S. V. Nair, K. Nishi, S. Sugou, T. Okuno, and Y. Masumoto, Phys. Rev. B **59**, R5300 (1999).
[17] S. Cortez, O. Krebs, P. Voisin, and J. M. Gerard, Phys. Rev. B **63**, 233306 (2001).
[18] G. Cantele, G. Piacente, D. Ninno, and G. Iadonisi, Phys. Rev. B **66**, 113308 (2002).
[19] K. Silverman, R. Mirin, S. Cundiff, and A. Norman, Appl. Phys. Lett. **82**, 4552 (2003).
[20] A. S. Saada, *Elasticity: Theory and Applications* (Pergamon Press, New York, 1974).
[21] C. Pryor, J. Kim, L.-W. Wang, A. J. Williamson, and A. Zunger, J. Appl. Phys. **83**, 2548 (1998).
[22] M. Grundmann, O. Stier, and D. Bimberg, Phys. Rev. B **52**, 11969 (1995).
[23] *Nano-Optoelectronics Concepts, Physics and Devices*, edited by M. Grundmann, (Springer, Berlin, 2002), Chap. 7.
[24] O. Stier, M. Grundmann, and D. Bimberg, Phys. Rev. B **59**, 5688 (1999).
[25] G. Pryor, Phys. Rev. B **57**, 7190 (1998).
[26] S. Hackenbuchner, M. Sabathil, J. Majewski, G. Zandler, P. Vogl, E. Beham, A. Zrenner, and P. Lugli, Physica B **314**, 145 (2002).
[27] P. N. Keating, Phys. Rev. **145**, 637 (1966).
[28] S. J. Jiang, Phys. Rev. B **56**, 4696 (1997).
[29] M. Cusack, P. Briddon, and M. Jaros, Phys. Rev. B **54**, R2300 (1996).
[30] T. Bahder, Phys. Rev. B **41**, 11992 (1990).
[31] O. Stier, *Electronic an Optical Properties of Quantum Dots and Wires* (Wissenschaft & Technik Verlag, Berlin, 2001).
[32] A. Zunger, Phys. Status Solidi B **224**, 727 (2001).
[33] R. Santoprete, B. Koiller, R. Capaz, P. Kratzer, Q. Liu, and M. Scheffler, Phys. Rev. B **68**, 235311 (2003).
[34] Y. Niquet, C. Delerue, G. Allan, and M. Lannoo, Phys. Rev. B **62**, 5109 (2000).
[35] G. Klimeck, F. Oyafuso, T. B. Boykin, R. Bowen, and P. von Allmen, Comput. Model. Eng. Sci. **3**, 601 (2002).
[36] V. Ranjan, G. Allan, C. Priester, and C. Delerue, Phys. Rev. B **68**, 115305 (2003).
[37] G. Bryant and W. Jaskolski, Phys. Rev. B **67**, 205320 (2003).
[38] A. J. Williamson, L.-W. Wang, and A. Zunger, Phys. Rev. B **62**, 12963 (2000).
[39] A. J. Williamson and A. Zunger, Phys. Rev. B **59**, 15819 (1999).
[40] R. Martin, Phys. Rev. B **5**, 1607 (1972).
[41] R. Resta, Rev. Mod. Phys. **66**, 899 (1994).
[42] N. Marzari and D. Vanerbilt, Phys. Rev. B **56**, 12847 (2002).
[43] S. Adachi, *Physical Properties of III–V Semiconductor Compounds* (Wiley, New York, 1992).
[44] W. H. Press, S. A. Teukolsky, W. T. Vetterling, and B. P. Flannery, *Numerical Recipes* (Cambridge University Press, Cambridge, 1992).
[45] L.-W. Wang and A. Zunger, Phys. Rev. B **59**, 15806 (1999).
[46] L. W. Wang, A. J. Williamson, A. Zunger, H. Jiang, and J. Singh, Appl. Phys. Lett. **76**, 339 (2000).
[47] S. Cortez, O. Krebs, and P. Voisin, J. Vac. Sci. Technol. B **18**, 2232 (2000).
[48] S. Cho, J. Kim, A. Sanz-Hervas, A. Majerfeld, G. Patriarche, and B. Kim, Phys. Status Solidi A **195**, 260 (2003).
[49] P. Ballet, P. Disseix, J. Leymarie, A. Vasson, A.-M. Vasson, and R. Grey, Thin Solid Films **336**, 354 (1998).
[50] C. H. Chan, M. C. Chen, H. H. Lin, Y. F. Chen, G. J. Jan, and Y. H. Chen, Appl. Phys. Lett. **72**, 1208 (1998).
[51] P. D. Berger, C. Bru, Y. Baltagi, T. Benyattou, M. Berenguer, G. Guillot, X. Marcadet, and J. Nagle, Microelectron. J. **26**, 827 (1995).
[52] J. L. Sanchezrojas, A. Sacedon, F. Gonzalezsanz, E. Calleja, and E. Munoz, Appl. Phys. Lett. **65**, 2042 (1994).
[53] T. B. Bahder, R. L. Tober, and J. D. Bruno, Phys. Rev. B **50**, 2731 (1994).
[54] R. L. Tober and T. B. Bahder, Appl. Phys. Lett. **63**, 2369 (1993).
[55] R. A. Hogg, T. A. Fisher, A. R. K. Willcox, D. M. Whittaker, M. S. Skolnick, D. J. Mowbray, J. P. R. David, A. S. Pabla, G. J. Rees, R. Grey, *et al.*, Phys. Rev. B **48**, 8491 (1993).
[56] A. S. Pabla, J. L. Sanchezrojas, J. Woodhead, R. Grey, J. P. R. David, G. J. Rees, G. Hill, M. A. Pate, P. N. Robson, R. A. Hogg, *et al.*, Appl. Phys. Lett. **63**, 752 (1993).
[57] M. A. Migliorato, A. G. Cullis, M. Fearn, and J. H. Jefferson, Physica E (Amsterdam) **13**, 1147 (2002).
[58] P. Yu and M. Cardona,